Analysis Cover Sheet

PREPARED FOR PROGRAM: EN530.418/619 Aerospace Structures		DATE: 12 / 06 / 2023
PREPARED BY: ALEX REN, JASON ZHONG, KYLE DALRYMPLE, DILAN FERREIRA	REVIEWED BY: DR. TOM DRAGONE	

ANALYSIS NAME:

WINGBOX STRUCTURAL ANALYSIS

OBJECTIVE:

DESIGN, ANALYZE, AND TEST WING BOX STRUCTURE

DEMONSTRATE ABILITY TO SUPPORT DESIGN LOAD OF 50 LB DISTRIBUTED LOAD AND 50 LB POINT LOAD AT END OF BOX BEAM

OPTIMIZE STRUCTURE FOR MAXIMUM STRENGTH-TO-WEIGHT RATIO

VERIFY FAILURE PREDICTIONS

ASSUMPTIONS:

NO MANUFACTURING FLAWS

BEAM CROSS-SECTION IS HOLLOW RECTANGLE

POINT LOAD OCCURS AT CORNER OF BOX BEAM

RESULTS:

PREDICTED FAILURE LOAD OF 500LB WITH WEIGHT OF 3.59LB FOR STRENGTH-TO-WEIGHT RATIO OF 139.1.

PREDICTED FAILURE AT BOLT CONNECTION WITH TEST STRUCTURE WITH NET SECTION FAILURE OF TOP SPAR CAP

TESTED MAXIMUM LOAD SUPPORTED OF 585.4LB WITH WEIGHT OF 3.168LB

FAILURE OCCURRED AT BOLT CONNECTION WITH TEST STRUCTURE WITH FASTENER SHEAR OF BOLT

BEARING YIELD OF SPAR CAP AT ROOT OBSERVED

BUCKLING OF BOTTOM SKIN PANEL OBSERVED

CONCLUSIONS:

IMPORTANCE OF INDIVIDUAL BOX BEAM COMPONENTS TO INCREASE STRENGTH WHILE MAINTAIN LOW WEIGHT

GAINED AN UNDERSTANDING OF WHICH SPECIFIC LOADS ARE SUPPORTED BY EACH BOX BEAM COMPONENT

MOST LIKELY FAILURE MODES IN THE JOINTS DUE TO NET-SECTION IN WING BOXES WITH SIMILARLY APPLIED LOAD

LEARNED HOW TO NAVIGATE THE MANUFACTURING OF WING BOX COMPONENTS AND FASTENING THE COMPONENTS TOGETHER

REFERENCES:

1. *MMPDS-01.pdf*
2. *Niu, Chunyun. (2011). Airframe stress analysis and sizing. Hong Kong : Los Angeles, Calif. :Conmilit Press ; Technical Book Co. [distributor],*
3. *www.boltdepot.com*
4. *WingBox Structure Specification Rev-.doc*

ATTACH BODY OF ANALYSIS

TABLE OF CONTENTS

1. INTRODUCTION

1.1 Objective

This report describes the design, analysis, and test results of the Wing Box designed and constructed by Alex Ren, Jason Zhong, Kyle Dalrymple, and Dilan Ferreira for the EN530.418/618 Aerospace Structures course. The Wing Box is a sub-scale cantilevered semi-monocoque structure fabricated using techniques typical to aerospace construction. The Wing Box will be tested to failure. The report will demonstrate the ability of the box beam to successfully bear the design load and optimize the structure for strength-to-weight ratio. Additionally, the report will verify the analysis methods used to obtain predictions by subjecting the Wing Box structure to a distributed load and point loading to failure.

1.2 Summary of Analysis Results

The design load condition of the Wing Box is a 50 lbf distributed load plus a 50 lbf point load. Table 1.2.1 lists the safety factors for the design load condition.

Table 1.2.1 Minimum Safety Factors for Design Load

Component	Load Type	Failure Mode	Safety Factor	Section
Top Skin	Shear	Yield Strength	8.79	Root
Top Skin	Shear	Ultimate Strength	8.07	Root
Bottom Skin	Shear	Yield Strength	7.03	Root
Bottom Skin	Shear	Ultimate Strength	8.07	Root
Bottom Skin	Compressive	Buckling	8.24	Root
Spar	Shear	Yield Strength	5.70	Root
Spar	Shear	Ultimate Strength	6.53	Root
Web	Shear	Yield Strength	30.58	Root
Web	Shear	Ultimate Strength	52.62	Root
Web	Shear	Buckling	75.19	Web
Top Spar Cap	Tensile	Yield Strength	43.18	Root
Top Spar Cap	Tensile	Ultimate Strength	38.82	Root
Top Spar Cap	Bearing	Joint	6.79	Root
Top Spar Cap	Net-Section	Joint	6.33	Root
Top Spar Cap	Shear-Out	Joint	6.48	Root
Bottom Spar Cap	Compressive	Yield Strength	25	Root
Bottom Spar Cap	Compressive	Buckling	9.22	Root
Top Clip	Tensile	Yield Strength	43.18	Root
Top Clip	Tensile	Ultimate Strength	38.82	Root
Bottom Clip	Compressive	Yield Strength	25	Root
Bottom Clip	Compressive	Buckling	41.08	Root
Bolt	Shear	Joint	92.59	Root
Rivet	Shear	Joint	11.21	Root

The expected failure load is 500 lbf total with a 50 lbf distributed load plus a 450 lbf point load. The failure mode is expected to be net-section failure in a top spar cap at the root of the Wing Box structure.

The mass of the structure is calculated to be 3.59 lbm with a strength-to-weight ratio of 139.1. Table 1.2.2 lists the safety factors for the failure load condition.

Table 1.2.2 Minimum Safety Factors for Failure Load

Component	Load Type	Failure Mode	Safety Factor	Section
Top Skin	Shear	Yield Strength	1.68	Root
Top Skin	Shear	Ultimate Strength	1.54	Root
Bottom Skin	Shear	Yield Strength	1.35	Root
Bottom Skin	Shear	Ultimate Strength	1.54	Root
Bottom Skin	Compressive	Buckling	1.30	Root
Spar	Shear	Yield Strength	1.08	Root
Spar	Shear	Ultimate Strength	1.23	Root
Web	Shear	Yield Strength	5.49	Root
Web	Shear	Ultimate Strength	9.45	Root
Web	Shear	Buckling	13.50	Web
Top Spar Cap	Tensile	Yield Strength	6.82	Root
Top Spar Cap	Tensile	Ultimate Strength	6.13	Root
Top Spar Cap	Bearing	Joint	1.07	Root
Top Spar Cap	Net-Section	Joint	1.00	Root
Top Spar Cap	Shear-Out	Joint	1.02	Root
Bottom Spar Cap	Compressive	Yield Strength	3.95	Root
Bottom Spar Cap	Compressive	Buckling	1.45	Root
Top Clip	Tensile	Yield Strength	6.82	Root
Top Clip	Tensile	Ultimate Strength	6.13	Root
Bottom Clip	Compressive	Yield Strength	3.95	Root
Bottom Clip	Compressive	Buckling	6.48	Root
Bolt	Shear	Joint	14.62	Root
Rivet	Shear	Joint	1.77	Root

1.3 Summary of Test Results

The mass of the box beam structure was measured at 3.618 lb. The actual failure load was measured at 585.4 lb. This results in a strength-to-weight ratio of 161.8. Failure occurred in the bolt which connected one of the top spar caps to the root interface. The bolt failed to shear. Additionally, there were signs of the beginning of bearing stress failure at the root of one of the top spar caps as well as signs of warping in the bottomskin.

Several changes were made to the analysis due to the test. First, the horizontal location of the point load was changed to the actual distance away from the center. The point load location was changed from 3" from center to 5/8" from center. The initial analysis assumed that the point load was located at the edge of the box beam for maximum torsional load. Second, panel buckling was added as an additional failure case. In the preliminary analysis, all skin loads were assumed to be purely shear. However, panel buckling is also a failure mode that needs to be considered, especially seeing that the skin had signs of warping. Finally, the additional stringer area due to the C shape of the spars were taken into account. The preliminary analysis assumed the spars would be a 2 in high wall along the length of the Wing Box. However, due to manufacturing needs, the spars became C-channels. The post-test analysis added the additional material into the lumped stringer areas.

1.4 Requirements

The requirements listed below define the different components in the Wing Box structure.

1.4.1 Root Interface Requirements

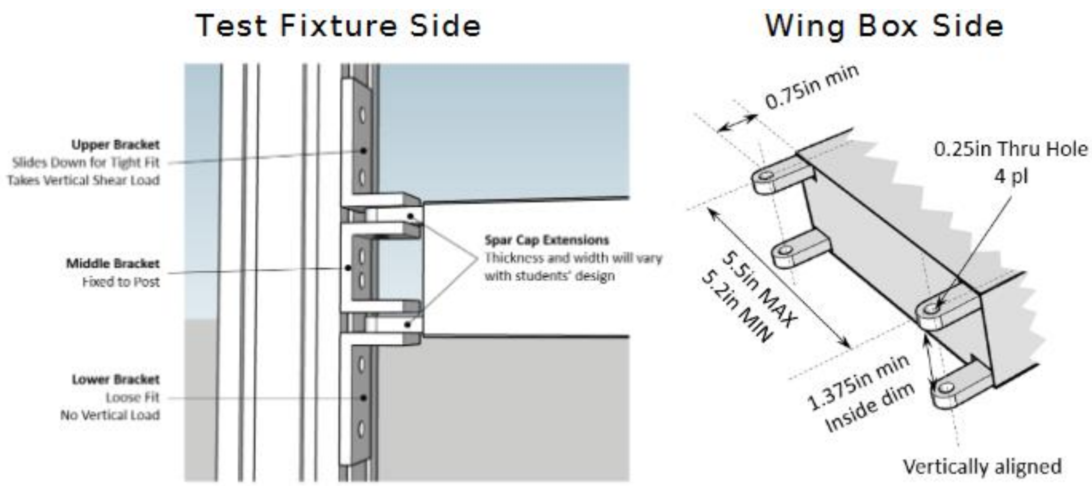

Figure 1.4.1.1 Root Interface Requirements

The Wing Box shall be attached to the test frame structure at its root with two pairs of vertically aligned holes in the spar caps. The root interface hole diameter shall be 0.25in nominally. The root interface holes shall be spaced chordwise between 5.2in and 5.5in. The root interface holes shall have a minimum spanwise spacing of 0.75in from the centerline of the hole to the inside face of the root rib. The inside gap between the upper face of the lower spar cap and the lower face of the upper spar cap shall be no less than 1.375in. The centerlines of the holes on upper and lower spar cap pairs shall be aligned vertically to within ±0.030in. The upper and lower pins in the root interface holes will share bending load. Only the upper pins will take vertical shear. There will be a vertical gap between the spar cap and the lower support, allowing the lower spar caps to slide vertically under load.

1.4.2 Tip Interface Requirements

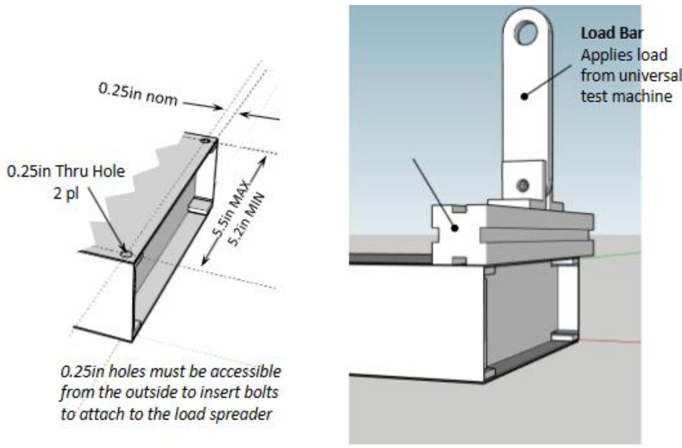

Figure 1.4.2.1 Tip Interface Requirements

The tip interface hole diameter shall be 0.25in nominally. The tip interface holes shall be spaced chordwise between 5.2in and 5.5in. The tip interface holes shall have a nominal spanwise location of 0.25in inboard of the outer edge of the upper skin/tip rib. The tip interface holes shall be accessible from the outboard side of the tip rib in order to insert the bolts to attach to the load spreader.

1.4.3 Geometry Requirements

The Wing Box Structure shall have a span of 16 ±0.5 in from the root rib surface to the tip rib surface (not including spar cap extensions for root and tip interfaces). The Wing Box Structure shall have a root chord of 6 ±0.25 in from the front spar to the rear spar, including all internal structures. The Wing Box Structure shall have a root height of 2 ±0.125 in from the bottom skin to the top skin, including all internal structures. The Wing Box Structure shall have a tip chord of 6 ±0.25 in from the front spar to the rear spar, including all internal structures. The Wing Box Structure may taper in height, but the tip height shall not exceed 2.125 in, including all internal structures. The Wing Box Structure skin and web thicknesses shall be between 0.020 in and 0.063 in thick, using the materials provided for this class. There are no restrictions on the Wing Box Structure spar cap dimensions, but the spar caps shall be made only from the materials provided for this class. Extruded and bar shapes may be modified at the students' discretion and based on their fabrication capabilities.

1.4.4 Performance Requirements

The Wing Box Structure shall be capable of supporting 50 lbf distributed load on its surface without yielding or permanent deformation. The distributed load will be applied to the surface of the Wing Box by a lead shot bag covering the surface. The Wing Box Structure shall be capable of supporting 50 lbf point load at its tip without yielding or permanent deformation. The point load will be applied by a universal test frame through the tip interface fixture. The point load may be applied at any chordwise station. The point load will be applied simultaneously with the distributed load. The Wing Box Structure shall be designed to function at room temperature, defined as 70°F ±10°F. The Wing Box Structure shall be designed to function at ambient pressure of 14.7 ±0.5 psia. The Wing Box Structure will not be subjected to random vibration or aero-acoustic loading, nor shock or explosive loading, nor repeated fatigue loading.

1.4.5 Design Factors

All components were designed with the factors listed in Table 1.4.5.1. Yield and ultimate factors apply to the design condition. Failure factors are used to determine the predicted capability of the structure.
Table 1.4.5.1

Table 1.4.5.1 Design Factors

Factor	**Yield**	**Ultimate**	**Failure**
Minimum Safety Factor	1.25	1.50	1.00
Buckling Factor	1.25	1.25	1.00
Fitting Factor	1.15	1.15	1.15

2. ASSEMBLY DESCRIPTION

2.1 Design

This section should describe the design of the structure. Include sketches of overall dimensions and critical interfaces and joints. Describe your rationale for making the design choices that you have made.

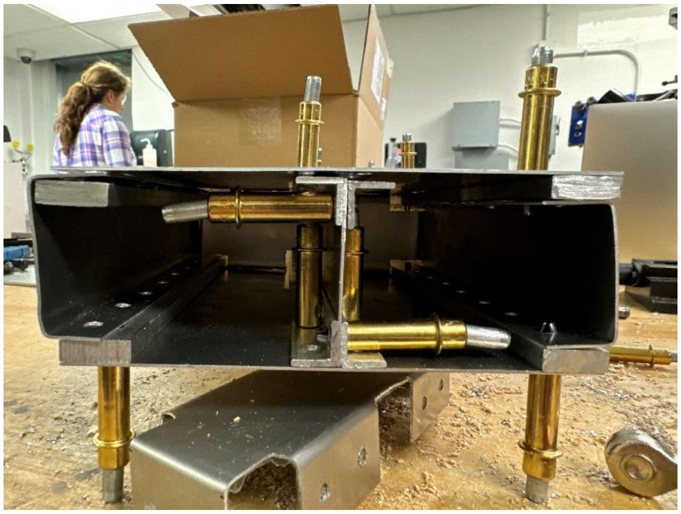

Figure 2.1.1 Overall View of the Aft Skirt Structural Assembly

The box beam structure consists of four rectangular spar caps, a single top skin panel, a single bottom skin panel, two side skin panels bent into a C shape, a single web, three ribs, and four stringers acting as clips.

The overall dimensions of the structure were chosen to be 6” wide, 2” tall, and 16” long in accordance with the required geometry.

Figure 2.1.2 Wing Box Structure Final Assembly

The spar caps were chosen to use the largest dimensions available of 0.75” W X 0.5” H (Fig.2.1.3) . These spar cap dimensions provided the largest area moment while requiring minimal manufacturing. As the analysis determined that the joint connection between the spar caps and the test rig would be the point of failure, the spar cap largest spar cap was chosen to maximize the load. Additionally, the chosen spar cap dimension was available as stock material for minimal manufacturing.

Figure 2.1.3 Wing Box Spar Cap

The top, bottom, and side skin panels as well as the web and rib were chosen to have the same thickness of 0.040”. This skin was chosen to resist shear flow within the safety factor while maintaining a lighter weight.

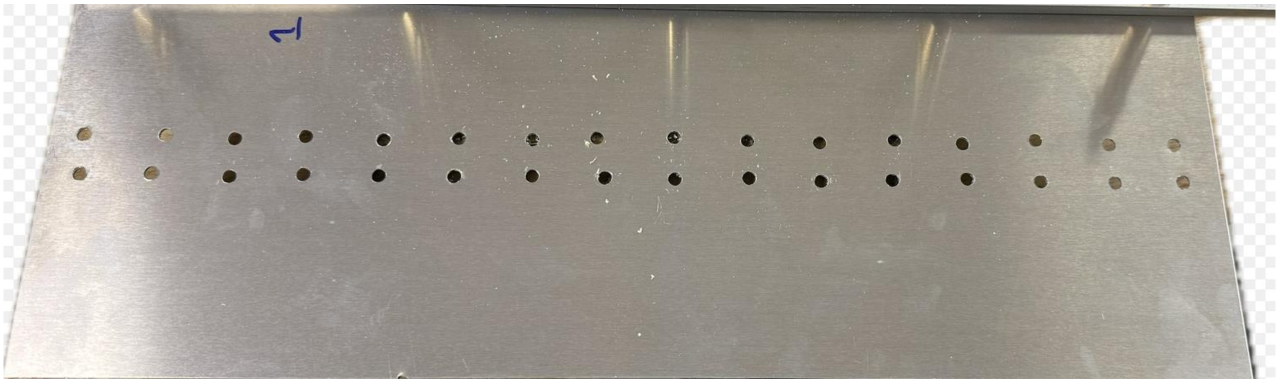

Figure 2.1.4 Wing Box Skin

The stringers were chosen to be right angle clips with a thickness of 3/16” and side lengths of 0.5”. These stringers were chosen to be these dimensions because we felt with the number of clips we included in our structure (a total of four), we could go for lighter clips to reduce the weight of the Wing Box.

Figure 2.1.5 Wing Box Stringers acting as clips

The ribs were placed at the root of the box beam and the tip of the box beam in accordance with the structure requirements. Additionally, a third rib was placed halfway between the root and tip at 8” from the root of the box beam structure. This placement was chosen to reduce dimpling in the top skin from the load.

The web was placed in the center of the cross-section of the box beam. This placement was chosen to assist resisting shear on the two side skin panels. The web was added to the box beam to help resist torsional loading under the assumption that the point load would be placed at the maximum distance from center which is 3”.

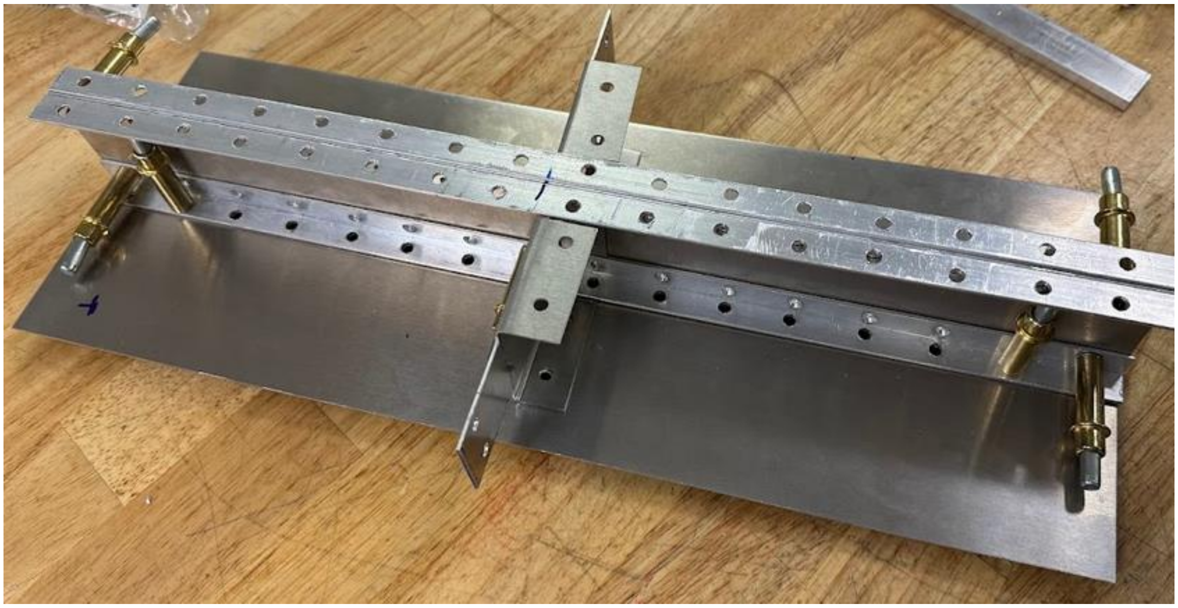

Figure 2.1.6 Wing Box Web with Ribs Attached

2.2 Fabrication

The first step in manufacturing was measuring and cutting the stringers, spar caps, and skins to size. After that was complete, holes were marked out on each piece and punched for ease of drilling. Once the holes were drilled, any parts that were to be match drilled were created. Assembling the structure using cleco's was the first step. This was to ensure that all the holes were lined up and did not need to be redrilled or bored out further due to accidental misalignment or warping. Once the structure had been fully assembled using cleco's, the riveting process could begin. Firstly, the central web was attached to the stringers, and then the inner ribs were bent and attached. Next, the skin panels were attached along with the spar caps and spars. The opposite side of spar caps and skin was then riveted to the existing structure. Something important to note was that when attaching multiple rivets all in a line, the rivets at the end were attached first, securing the two parts together. Then, additional rivets were added in alternating order between the two ends as to maximize the symmetry of any offsetting tensions due to poor manufacturing tolerances. Finally, the outer rib panels were attached the to ends of the box beam and the structure was complete. In order to keep like parts from being confused with one another marks were made and were used to ensure proper alignment.

Figure 2.2.1

Left to Right, Top to Bottom: Using cleco's to assemble the rough structure; Ensuring stringers are aligned with central web using cleco's; Assembling web, ribs, and stringers; Riveting skins, alternating from side to side; Completed Wing box; Final Trimming of Wing box.

2.3 Test

The test was conducted using an the Universal Testing Machine (UTM) in the JHU MBD Lab. The box beam was connected to the test frame by a tip interface and a root interface (Fig.2.3.1).

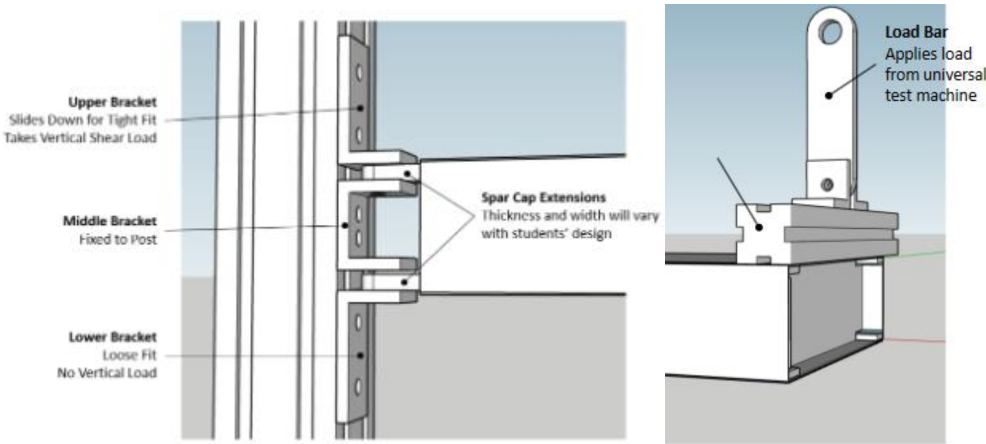

Figure 2.3.1 (Left) Root interface and (Right) tip interface

The tip interface consists of an 80-20 extrusion which attaches to the tip of the Wing Box through a ¼-20" screw. Right-angle brackets are used to secure the load bar of the LVDT to the extrusion. A pin keeps the load bar between the right-angle brackets.

The root interface consists of three brackets on each side of the box beam. The top spar cap is secured between the upper bracket and middle bracket while the bottom spar cap is secured between the lower bracket and middle bracket. ¼"-20 nuts and bolts are used to secure the spar caps between the brackets.

A protective screen was placed on the UTM to ensure that no injury occurred from potential flying objects.

A distributed load was applied through two 25 lbm lead bags. The distributed load was applied before the point load. The lead bags were laid on the box beam such that the total 50 lbm would be evenly distributed across the length of the box.

A point load was applied through the load bar of the LVDT cross head. After the distributed load was placed, the LVDT cross head applied the load by displacing the tip of the box beam downwards at a constant velocity. The point load was increased until the structure failed.

The load was measured through a load cell in the LVDT cross head and the displacement was measured by the position of the cross head. The measurements were recorded using LabVIEW and saved in an excel sheet.

3. ANALYSIS

3.1 Load Cases

Two load cases were analyzed which were the design load and the predicted failure load. The design load consisted of a 50 lbf distributed load and a 50 lbf point load at the tip of the Wing Box structure (Fig.3.1.1). The predicted failure load consisted of a 50 lbf distributed load and a 450 lbf point load at the tip of the Wing Box structure (Fig.3.1.2).

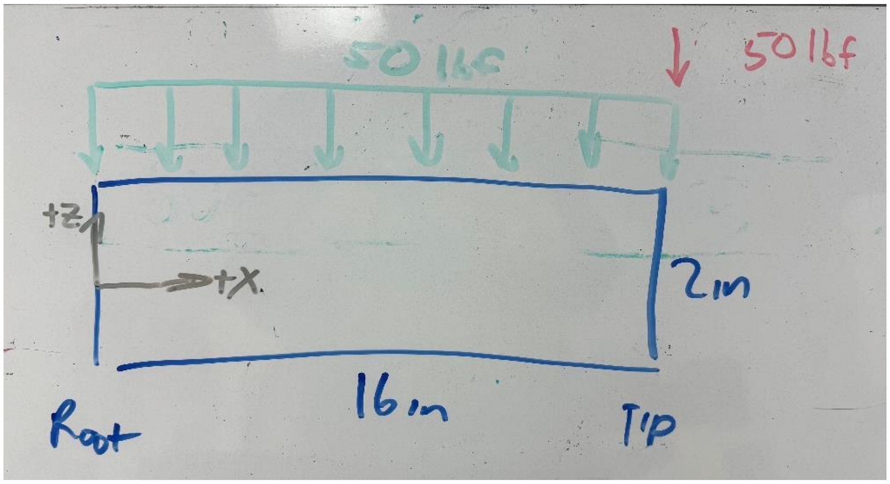

Figure 3.1.1 Design load condition of box beam

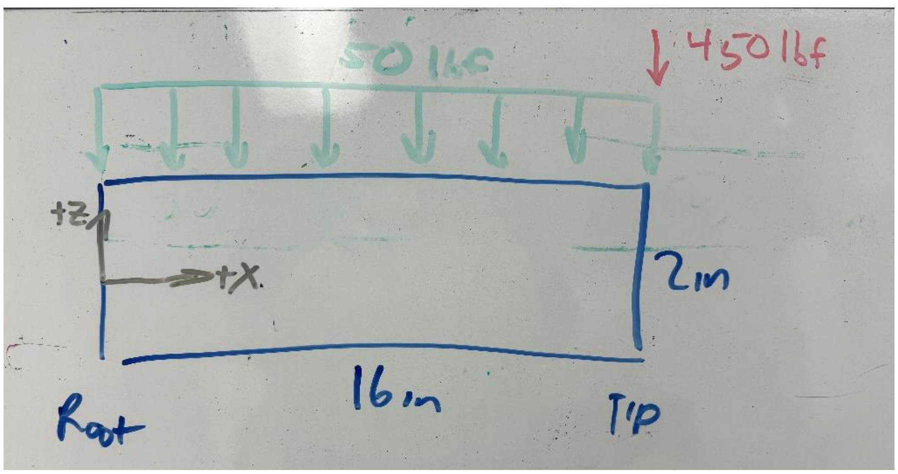

Figure 3.1.2 Failure load condition of box beam

3.2 Material Properties

The box beam used two different types of material. The skins, ribs, and web used Al5052-H32 in the form of a sheet while the spar caps and clips used Al6061-T6. The spar caps were extruded bars while the clips were an extruded shape. The material properties for Al5052-H32 were taken from MMPDS Table 3.5.1.0 and the material properties for Al6061-T6 were taken from MMPDS Table 3.2.6.0. The properties are summarized in Table 3.2.1 below.

Table 3.2.1 Material Properties

Property	**Skins, Ribs, Webs**	**Spar Caps, Clips**
Alloy and Temper	Al5052-H32	Al6061-T6
Form	Sheet	Extruded rod, bar, and shapes
Reference, MIL-HDBK-5H Table	3.5.1.0 AMS 4016	3.2.6.0 AMS 4150
Thickness *inches*	0.04	<1.000
Basis	S	B
Tensile Modulus *Msi*	10.1	9.9
Compressive Modulus *Msi*	10.2	10.1
Shear Modulus *Msi*	3.85	3.8
Poisson Ratio	0.33	0.33
Density *lbm/in*^{3}	0.097	0.098
Ultimate Tensile Strength (L) *ksi*	31	41
Ultimate Tensile Strength (LT) *ksi*	31	40
Tensile Yield Strength (L) *ksi*	23	38
Tensile Yield Strength (LT) *ksi*	22	36
Compressive Yield Strength (L) *ksi*	22	37
Compressive Yield Strength (LT) *ksi*	23	38
Ultimate Shear Strength (L) *ksi*	19	28
Shear Yield Strength (L) *ksi*	13.8	25.7
Ultimate Bearing Strength (e/D=2.0) *ksi*	65	88
Yield Bearing Strength (e/D=2.0) *ksi*	37	65

Two types of fasteners were used in the box beam. The first was a rivet which had a diameter of 3/16”. The second was a ¼”-20 bolt that was used to connect the root of the box beam to the test interface. The material of the rivet was aluminum with an aluminum mandrel and the properties were taken from the vendor’s website. While the material of the bolt was unknown, it is assumed to be made of AN Steel and the properties are found in Figure 9.2.7 in the *Airframe Stress Analysis and Sizing* textbook by Michael C. Y. Niu. The properties of the fasteners are summarized in Table 3.2.2 below.

Table 3.2.2 Fastener Properties

Property	**Rivets**	**Bolts**
Material	Aluminum-Aluminum Mandrel	AN Steel
Reference, Product Catalog	www.boltdepot.com	Fig 9.2.7 Airframe Stress Analysis and Sizing by Michael C. Y. Niu
Diameter *inches*	0.19	0.25
Nominal Hole Diameter *inches*	0.191	0.25
Tensile Strength *lbs*	320	4080
Shear Strength *lbs*	260	3680

3.3 Analysis Methods

Analytical methods for the box beam included stress analysis using the box beam method, strength failure analysis, buckling analysis, and joint analysis.

3.3.1 Stresses from Box Beam Method

Due to the inclusion of a web, a two-cell box beam analysis was required to calculate the axial loads in the spar caps and clips as well as the shear loads in the skins and webs.

The first step of the analysis was to determine the reaction force at the root of the box beam due to the design distributed load and point load. The input point load of 50lbf was combined with the input distributed load of 50lbf to determine the reaction moment and reaction vertical load at the root of the box beam.

With the reaction moment and forces calculated, the next step was to calculate the shear and moment in the box beam at different points along the beam. A shear and moment diagram were produced from these calculations.

The design of the box beam was idealized into a two-cell lumped stringer model with six nodes (Fig.3.3.1.1). The lumped stringer model was used to find the center of gravity and the area moments of inertia of the Wing Box.

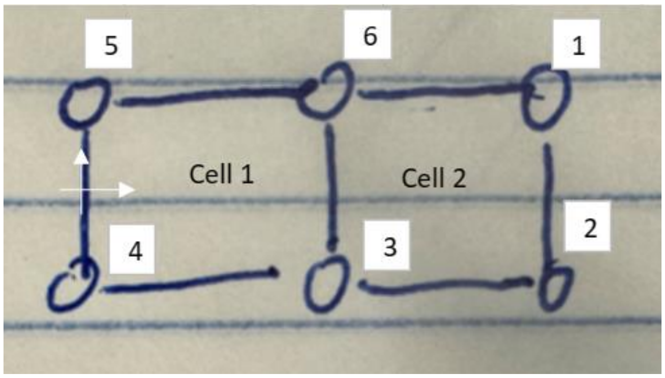

Figure 3.3.1.1 Lumped stringer idealization of box beam.

Next, the shears and moments calculated previously are used in conjunction with the inertia calculations to determine the axial stress and axial load on the lumped stringer node at each of the rib locations.

After calculating the axial stresses, the shear stresses were calculated. This was done by calculating the cut web shear flow and the torque unbalance shear flows to determine the total shear flow and shear stress in each web. Due to the two-cell design, additional equations for the angle of twist of each cell were required to determine the shear stresses.

The steps for analyzing the stresses for a two-cell box beam are additionally described in Example 3 of Chapter 8 in *Airframe Stress Analysis and Sizing* by Michael C. Y. Niu.

3.3.2 Strength Failure

Safety factors against yield and ultimate strength failure in every component in the box beam were computed using the formula:

$$SF_{STRENGTH} = \frac{F_{all}}{F_{ind}} \qquad \textit{(Eq. 3.3.2.1)}$$

Where $SF_{STRENGTH}$ is the strength safety factor, F_{all} is the allowable stress (including yield/ultimate design factors where appropriate) and F_{ind} is the induced stress which the component experiences. The allowable stress can be tensile strength, compressive strength, or shear strength depending on the load type.

The safety factor was then compared to the minimum safety factor required as listed in Table 1.4.5.1 to determine whether the design was adequate.

3.3.3 Buckling Failure

Buckling failure analysis was conducted for several components in the box beam. Compressive buckling analysis was done for the skin panels as well as the clips and spar caps. Shear buckling analysis was required for the web.

Safety factors against buckling failure were computed using Eq.3.2.2.1.

The safety factor was then compared to the minimum safety factor required as listed in Table 1.4.5.1 to determine whether the design was adequate.

For the skin panel buckling, a compression panel analysis was done. The skin panel was analyzed using four clamped sides. Figure 11.3.1 in *Airframe Stress Analysis and Sizing* was used to determine the K_c compression buckling coefficient of the panel. Critical elastic buckling stress was computed with the formula:

$$\frac{F_{c,cr}}{\eta_c} = K_c E \left(\frac{t}{b}\right)^2 \qquad \textit{(Eq. 3.3.3.1)}$$

Where $F_{c,cr}$ is the critical buckling stress, η_c is the plasticity reduction factor in compressive load, E is the Young's Modulus of the material, t is the thickness of the material, and b is the short length of the panel. Figure 11.2.4 in *Airframe Stress Analysis and Sizing* was then used to determine $F_{c,cr}$. Allowable stress was then determined with the formula:

$$\sigma_{all} = \frac{F_{c,cr}}{DF_{buckling}} \qquad \textit{(Eq. 3.3.3.2)}$$

Where σ_{all} is the allowable stress and $DF_{buckling}$ is the buckling design factor. The induced stress is found by taking the maximum axial stress on the panel which occurs at the root of the box beam.

For the web shear buckling, a shear panel analysis was done. The analysis was done using four clamped sides. Figure 11.3.5 in *Airframe Stress Analysis and Sizing* was used to determine the K_s shear buckling coefficient for in-plane shear. The critical elastic buckling stress was calculated using the formula:

$$\frac{F_{s,cr}}{\eta_s} = K_s E \left(\frac{t}{b}\right)^2 \qquad \textit{(Eq. 3.3.3.3)}$$

Where $F_{s,cr}$ is the critical buckling stress and η_s is the plasticity reduction factor in shear load. Figure 11.2.4 in *Airframe Stress Analysis and Sizing* was then used to determine $F_{s,cr}$. Allowable stress was then determined with the formula:

$$\sigma_{all} = \frac{F_{s,cr}}{DF_{buckling}} \quad \textit{(Eq. 3.3.3.4)}$$

The induced stress is the shear stress on the web found in the box beam analysis.

The clips and spar caps both were analyzed using Euler buckling. Both were considered Pinned-Pinned ends for a column end fixity of 1. First, the moments of inertia for each component were calculated as well as the cross-sectional area. Next, the radius of gyration was calculated using the formula:

$$\rho = \sqrt{\frac{I}{A}} \quad \textit{(Eq. 3.3.3.5)}$$

Because the column end fixity is 1, the slenderness ratio can be calculated using the formula:

$$SR = \frac{L}{\rho} \quad \textit{(Eq. 3.3.3.6)}$$

Where SR is the slenderness ratio and L is the length of the beam. A large slenderness ratio is used to confirm the use of Euler buckling analysis. The allowable stress is then calculated by using the formula:

$$f_{cr} = \frac{c\pi^2 E}{\left(\frac{L}{\rho}\right)^2} \quad \textit{(Eq. 3.3.3.7)}$$

Where $f_{cr}$is the allowable stress. The induced stress is found from the box beam analysis of axial stresses.

3.3.4 Joint Failure

Safety factors against buckling failure were computed using Eq.3.2.2.1.

The safety factor was then compared to the minimum safety factor required as listed in Table 1.4.5.1 to determine whether the design was adequate.

Four failure modes were considered for the analysis of the rivets and bolts. These failure modes are bolt/rivet shear, bearing, net section, and shear out failure.

The allowable stress for bolt/rivet shear was found using the fastener properties listed in Table 1.4.5.1.

The allowable stress for bearing failure was calculated using the formula:

$$f_{bearing} = \frac{F_{bru} t D}{DF_{fitting}} \quad \textit{(Eq. 3.3.4.1)}$$

Where $f_{bearing}$ is the allowable bearing stress, F_{bru} is the sheet ultimate bearing strength, t is the sheet thickness, D is the fastener diameter, and $DF_{fitting}$ is the fitting design factor.

The allowable stress for net-section failure was calculated using the formula:

$$f_{net} = \frac{F_{tu}(p - D)t}{DF_{fitting}} \qquad \textit{(Eq. 3.3.4.2)}$$

Where f_{net} is the allowable net-section stress, F_{tu} is the sheet ultimate tensile strength, and p is the hole spacing.

The allowable stress for shear out failure was calculated using the formula:

$$f_{shear} = 2F_{su}et \qquad \textit{(Eq. 3.3.4.3)}$$

Where f_{shear} is the allowable shear-out stress, F_{su} is the sheet ultimate shear strength, and e is the edge spacing of the hole.

The induced stresses were found from the maximum axial loads from the box beam analysis.

4. ANALYSIS RESULTS

The results of the analysis show a minimum safety factor of 6.33 under the design load. The failure load is determined to be a total load of 500 lbf with 450 lbf point load and 50 lbf distributed load. Failure occurs due to net section failure in the top spar cap at root interface. With a calculated weight of 3.59 lbm, this results in a predicted strength-to-weight ratio of 139.1.

4.1 Stresses from Box Beam Analysis

To analyze the box beam, the box beam design is simplified to a lumped stringer model as seen in Figure 4.1.1.

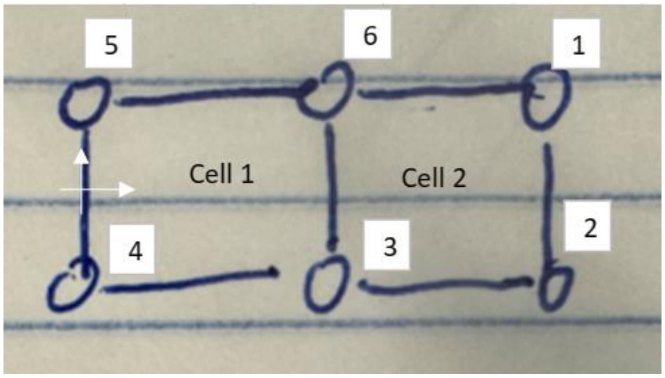

Figure 4.1.1 Lumped stringer idealization of box beam.

Using the design load, the reaction forces are found to be as follows in Table 4.1.1. This results in the shear and moment diagrams in Figure 4.1.2.

Table 4.1.1 Reaction Forces at Root Under Design Load

Reaction Type	Load
Moment (M_x)	-1200 in-lbf
Force (R_z)	100 lbf

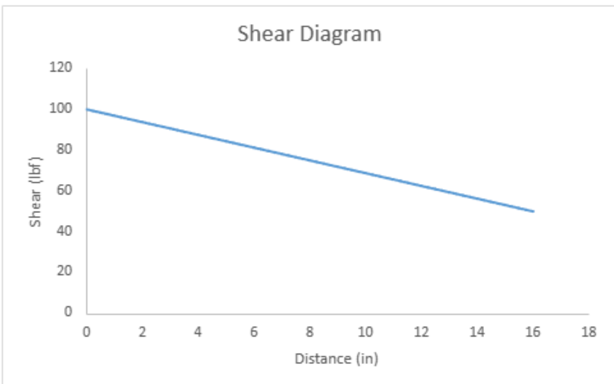

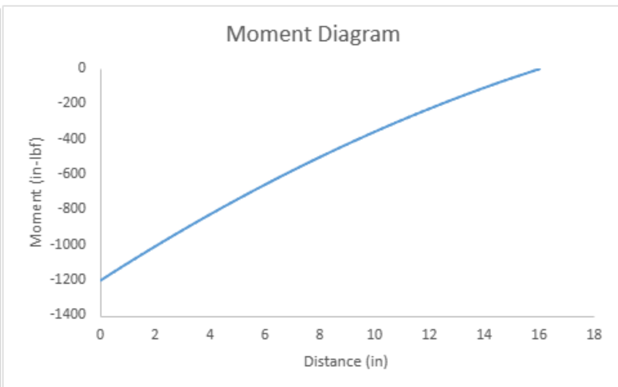

Figure 4.1.2 (Left) Shear and (Right) Moment Diagrams Under Design Load Conditions

Using the multicell box beam method, the resulting axial stresses in the lumped stringer are found in Table 4.1.2 and the resulting shear stresses in the skin are found in Table 4.1.3.

Table 4.1.2 Lumped Stringer Axial Stresses Under Design Load

Stringer Number	Load Type	X-Location (in)	Resulting Stress (psi)
1	Tensile	0	704
2	Compressive	0	-704
3	Compressive	0	-704
4	Compressive	0	-704
5	Tensile	0	704
6	Tensile	0	704
1	Tensile	8	293
2	Compressive	8	-293
3	Compressive	8	-293
4	Compressive	8	-293
5	Tensile	8	293
6	Tensile	8	293
1	None	16	0
2	None	16	0
3	None	16	0
4	None	16	0
5	None	16	0
6	None	16	0

Table 4.1.3 Lumped Stringer Model Shear Stresses Under Design Load

Web Number	Load Type	X-Location (in)	Resulting Stress (psi)
12(web)	Shear	0-8	484
23	Shear	0-8	853
34	Shear	0-8	1569
45(web)	Shear	0-8	1938
56	Shear	0-8	1569
61	Shear	0-8	853
36(web)	Shear	0-8	361
12(web)	Shear	8-16	301
23	Shear	8-16	564
34	Shear	8-16	1076
45(web)	Shear	8-16	1340
56	Shear	8-16	1076
61	Shear	8-16	564
36(web)	Shear	8-16	258

Using the calculated failure load results in the reaction forces in Table 4.1.4 and the shear and moment diagrams in Figure 4.1.3.

Table 4.1.4 Reaction Forces at Root Under Failure Load

Reaction Type	Load
Moment (M_x)	-7600 in-lbf
Force (R_y)	500 lbf

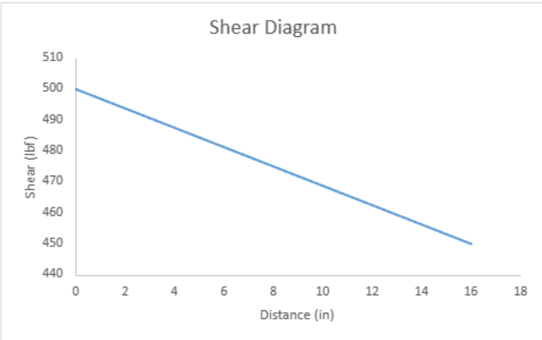

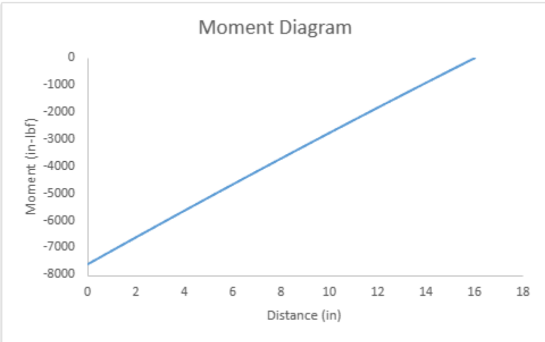

Figure 4.1.3 (Left) Shear and (Right) Moment Diagrams Under Failure Load Conditions

The axial stresses in the failure load condition are significantly higher than the design load condition (Table 4.1.5). The same holds true for the shear stresses (Table 4.1.6).

Table 4.1.5 Lumped Stringer Axial Stresses Under Design Load

Stringer Number	Load Type	X-Location (in)	Resulting Stress (psi)
1	Tensile	0	4459
2	Compressive	0	-4459
3	Compressive	0	-4459
4	Compressive	0	-4459
5	Tensile	0	4459
6	Tensile	0	4459
1	Tensile	8	2171
2	Compressive	8	-2171
3	Compressive	8	-2171
4	Compressive	8	-2171
5	Tensile	8	2171
6	Tensile	8	2171
1	None	16	0
2	None	16	0
3	None	16	0
4	None	16	0
5	None	16	0
6	None	16	0

Table 4.1.6 Lumped Stringer Model Shear Stresses Under Design Load

Web Number	Load Type	X-Location (in)	Resulting Stress (psi)
12(web)	Shear	0-8	2158
23	Shear	0-8	4214
34	Shear	0-8	8208
45(web)	Shear	0-8	10264
56	Shear	0-8	8208
61	Shear	0-8	4214
36(web)	Shear	0-8	2012
12(web)	Shear	8-16	1975
23	Shear	8-16	3926
34	Shear	8-16	7715
45(web)	Shear	8-16	9665
56	Shear	8-16	7715
61	Shear	8-16	3926
36(web)	Shear	8-16	1908

4.2 Strength Failure

Table 4.2.1 shows the stresses, allowable loads, and calculated safety factors for strength failure under the design load condition. Under the design load, none of the components fail in terms of strength as the safety factors are all greater than the design factors.

Table 4.2.1 Strength Failure Stresses, Allowable Loads, Safety Factors and Design Factors Under Design Load

Component	Load Type	Induced Stress (psi)	Allowable Stress (psi)	Safety Factor	Design Factor
Top Skin Panel	Shear Yield	1569	13800	8.79	1.25
Top Skin Panel	Shear Ultimate	1569	12667	8.07	1.5
Bottom Skin Panel	Shear Yield	1569	11040	7.03	1.25
Bottom Skin Panel	Shear Ultimate	1569	12667	8.07	1.5
Spar	Shear Yield	1938	11040	5.70	1.25
Spar	Shear Ultimate	1938	12667	6.53	1.5
Web	Shear Yield	361	11040	30.58	1.25
Web	Shear Ultimate	361	19000	52.62	1.5
Top Spar Cap	Tensile Yield	704	30400	43.18	1.25
Top Spar Cap	Tensile Ultimate	704	27333	38.82	1.5
Bottom Spar Cap	Compressive Yield	-704	-17600	25.00	1.25
Top Clip	Tensile Yield	704	30400	43.18	1.25
Top Clip	Tensile Ultimate	704	27333	38.82	1.5
Bottom Clip	Compressive Yield	-704	-17600	25.00	1.25

No components fail in terms of strength either as all safety factors are greater than the failure design factor although the spar is close to yielding. Table 4.2.2 shows the stresses, allowable loads, and calculated safety factors for strength failure under the failure load condition.

Table 4.2.2 Strength Failure Stresses, Allowable Loads, Safety Factors and Design Factors Under Failure Load

Component	Load Type	Induced Stress (psi)	Allowable Stress (psi)	Safety Factor	Design Factor
Top Skin Panel	Shear Yield	8208	13800	1.68	1
Top Skin Panel	Shear Ultimate	8208	12667	1.54	1
Bottom Skin Panel	Shear Yield	8208	11040	1.35	1
Bottom Skin Panel	Shear Ultimate	8208	12667	1.54	1
Spar	Shear Yield	10264	11040	1.08	1
Spar	Shear Ultimate	10264	12667	1.23	1
Web	Shear Yield	2012	11040	5.49	1
Web	Shear Ultimate	2012	19000	9.45	1
Top Spar Cap	Tensile Yield	4459	30400	6.82	1
Top Spar Cap	Tensile Ultimate	4459	27333	6.13	1
Bottom Spar Cap	Compressive Yield	-4459	-17600	3.95	1
Top Clip	Tensile Yield	4459	30400	6.82	1
Top Clip	Tensile Ultimate	4459	27333	6.13	1
Bottom Clip	Compressive Yield	-4459	-17600	3.95	1

4.3 Buckling Failure

Buckling analysis was conducted on the web, the skin panel, the spar caps, and the clips. The allowable stress for the skin panel and web were analyzed using panel buckling analysis (Table 4.3.1) and the allowable stress for the spar caps and clips were analyzed using Euler buckling analysis (Table 4.3.2)

Table 4.3.1 Panel Buckling Allowable Stress

Component	a/b	K	$\frac{F_{cr}}{\eta}$ (psi)	F_{cr} (psi)	Allowable Stress (psi)
Skin Panel	2.67	4	7200	7200	5800
Web	4	8.4	33900	33900	27100

Table 4.3.2 Euler Buckling Allowable Stress

Component	c	I (in^4)	A (in^2)	ρ (in)	Slenderness Ratio	F_{cr} (psi)	Allowable Stress (psi)
Spar Cap	1	0.000977	0.1875	0.07	110.8	8100	6500
Clip	1	0.00136	0.058	0.15	52.5	36200	28900

Using the design load, none of the components fail due to buckling. All the safety factors were above the minimum safety design factors (Table 4.3.3)

Table 4.3.4 Buckling Failure Stresses, Allowable Loads, Safety Factors and Design Factors Under Design Load

Component	Load Type	Induced Stress (psi)	Allowable Stress (psi)	Safety Factor	Design Factor
Skin Panel	Compression Panel	-704	5800	8.24	1
Web	Shear Panel	361	27100	75.19	1
Spar Cap	Euler Buckling	-704	6500	9.21	1
Clip	Euler Buckling	-704	28900	40.08	1

No components fail due to buckling under the failure condition either, although some components like the skin panel come very close. All the safety factors were above the minimum failure design factors (Table 4.3.4)

Table 4.3.4 Buckling Failure Stresses, Allowable Loads, Safety Factors and Design Factors Under Failure Load

Component	Load Type	Induced Stress (psi)	Allowable Stress (psi)	Safety Factor	Design Factor
Skin Panel	Compression Panel	-4459	5800	1.30	1
Web	Shear Panel	2012	27100	13.50	1
Spar Cap	Euler Buckling	-4459	6500	1.46	1
Clip	Euler Buckling	-4459	28900	6.48	1

4.4 Joint Failure

Joint analysis was conducted for both the root bolt and the root rivets. Only the root rivets were analyzed as they would be under the highest stress. Table 4.4.1 summarizes the design parameters for each joint.

Table 4.4.1 Sheet and Fastener Parameters

Component	Parameter	Value
Bolt Sheet	Ultimate Shear Strength	28 ksi
Bolt Sheet	Ultimate Tensile Strength	41 ksi
Bolt Sheet	Ultimate Bearing Strength	88 ksi
Bolt Sheet	Thickness	0.25 in
Bolt	Hole Diameter	0.25 in
Bolt	Hole Spacing	0.75 in
Bolt	Edge Spacing	0.375 in
Bolt	Ultimate Shear Force	3680 lbf
Bolt	Ultimate Shear Stress	75 ksi
Rivet Sheet	Ultimate Shear Strength	28 ksi
Rivet Sheet	Ultimate Tensile Strength	41 ksi
Rivet Sheet	Ultimate Bearing Strength	88 ksi
Rivet Sheet	Thickness	0.33 in
Rivet	Hole Diameter	0.191 in
Rivet	Hole Spacing	1 in
Rivet	Edge Spacing	0.375 in
Rivet	Ultimate Shear Force	260 lbf
Rivet	Ultimate Shear Stress	9.1 ksi
All	Fitting Factor	1.15

These parameters were used to calculate the allowable stresses for each failure mode. Using the design load, all the failure modes are above the minimum safety design factor and will not fail. Table 4.4.2 shows the resulting stresses, allowable stresses, and safety factors for the joints.

Table 4.4.2 Joint Failure Stresses, Allowable Loads, Safety Factors and Design Factors Under Design Load

Component	Failure Mode	Induced Stress (psi)	Allowable Stress (psi)	Safety Factor	Design Factor
Bolt	Shear	704	65190	92.59	1.5
Top Spar Cap (Bolt "Sheet")	Bearing	704	4783	6.79	1.5
Top Spar Cap (Bolt "Sheet")	Net Section	704	4457	6.33	1.5
Top Spar Cap (Bolt "Sheet")	Shear Out	704	4565	6.48	1.5
Rivet	Shear	704	7891	11.21	1.5
Top Spar Cap (Rivet "Sheet")	Bearing	704	4823	6.85	1.5
Top Spar Cap (Rivet "Sheet")	Net Section	704	9518	13.52	1.5
Top Spar Cap (Rivet "Sheet")	Shear Out	704	6026	8.56	1.5

Using calculated failure load, the top spar cap will fail due to net-section failure. This failure leads to the failure of the entire box beam. The safety factor of the top spar cap under net-section failure is 1, which is the failure minimum safety factor. Table 4.4.3 shows the resulting stresses, allowable stresses, and safety factors for the joints.

Table 4.4.3 Joint Failure Stresses, Allowable Loads, Safety Factors and Design Factors Under Failure Load

Component	Failure Mode	Induced Stress (psi)	Allowable Stress (psi)	Safety Factor	Design Factor
Bolt	Shear	4459	65190	14.62	1
Top Spar Cap (Bolt "Sheet")	Bearing	4459	4783	1.07	1
Top Spar Cap (Bolt "Sheet")	Net Section	4459	4457	1.00	1
Top Spar Cap (Bolt "Sheet")	Shear Out	4459	4565	1.02	1
Rivet	Shear	4459	7891	1.77	1
Top Spar Cap (Rivet "Sheet")	Bearing	4459	4823	1.08	1
Top Spar Cap (Rivet "Sheet")	Net Section	4459	9518	2.13	1
Top Spar Cap (Rivet "Sheet")	Shear Out	4459	6026	1.35	1

4.5 Mass Estimate

The mass estimate was found by estimating the volume of the skins, webs, ribs, spar caps, and clips used in the structure and multiplying by the respective densities of materials. In addition, the mass of the rivets was included by estimating the total number of rivets and multiplying by the mass of each rivet. Table 4.5.1 shows the calculated masses of each component as well as the total mass of the structure.

Table 4.5.1 Mass Estimate

Component	Volume (in^3)	Mass (lbm)	Quantity
Clip	0.9375	0.092	4
Spar Cap	3	0.29	4
Skin Panel	3.84	0.37	2
Spar	1.28	0.12	2
Web	1.28	0.12	1
Rib	0.48	0.046	3
Rivets	-	0.0041	200
Total	-	3.59	-

5. TEST RESULTS

Alignment issues occurred in the setup of the box beam in the testing aparatus. The root interface holes were not within the alignment tolerance. Fig.5.1 shows the box beam installed in the testing aparatus before the initiation of the test. The point load was applied 5/8" from the center of the box beam.

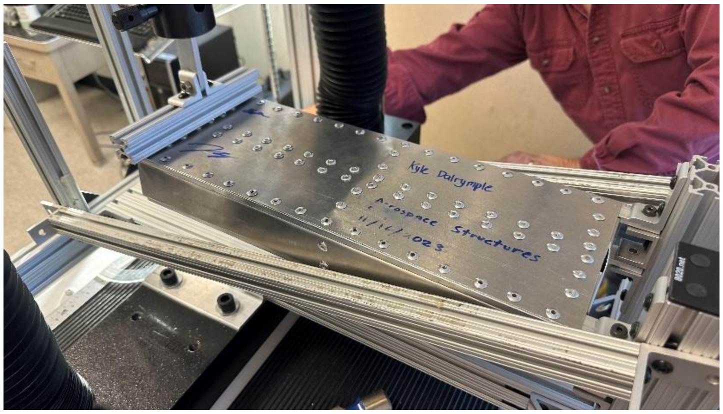

Figure 5.1 Box beam installed in testing apparatus before loading

Three trials occurred before the final test where the point load was incorrectly loaded in the opposite direction. These trials went up to a maximum load of between 100-200 lbf each trial.

During the test, the box beam remained very rigid and did not experience much deformation except at the root interface (Fig.5.2).

Figure 5.2 Box beam in middle of test. The beam itself shows little deformation and remains straight although deflection is high.

Figure 5.3 shows the relationship between the tip deflection and the load applied.

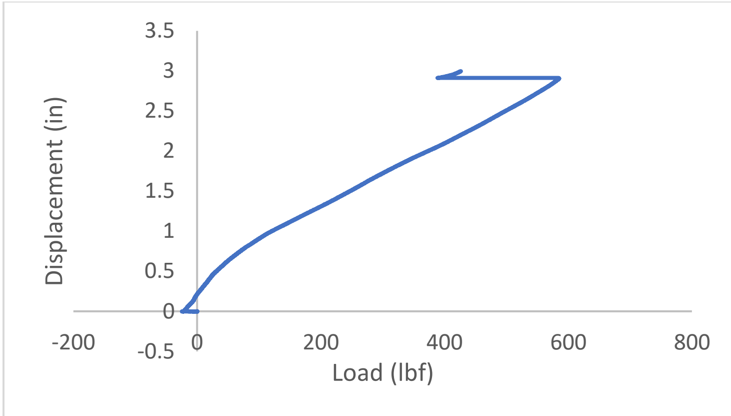

Figure 5.3 Plot of Displacement vs Load.

The test ended with the failure of the bolt connection at the root interface (Fig.5.4). The failure mode was bolt shear at a load of 585.4 lbf (Fig.5.5). This was a higher load than predicted, which was 500lbf. Additionally, the mode of failure was different. The failure mode was bolt shear rather than the predicted net section failure in the top spar cap. The location of failure was the same, as both the predicted and actual failure occurred at the root interface and involved the joint.

Figure 5.4 Bolt shear failure

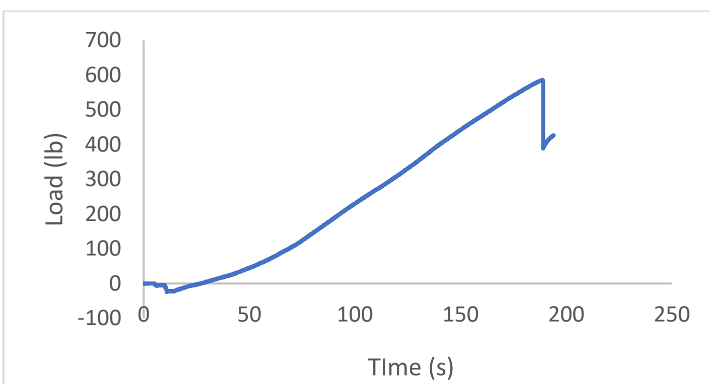

Figure 5.5 Plot of Load vs Time. Maximum load of 585.4lbf reached.

After the test, there were visible signs of buckling in the skin panel as well as the beginning of bearing yield in the top spar cap at the root connection (Fig.5.6).

Figure 5.6 (Left) Buckling of skin and (Right) bearing yielding at end of test

The maximum predicted deflection was a deflection of 0.000021” which was much less than the actual deflection of 3.00” (Fig.5.7). This could be due to the much smaller moment of inertia at the root interface. Additionally, the improper attachment to the test apparatus may have contributed to the significant difference in deflection.

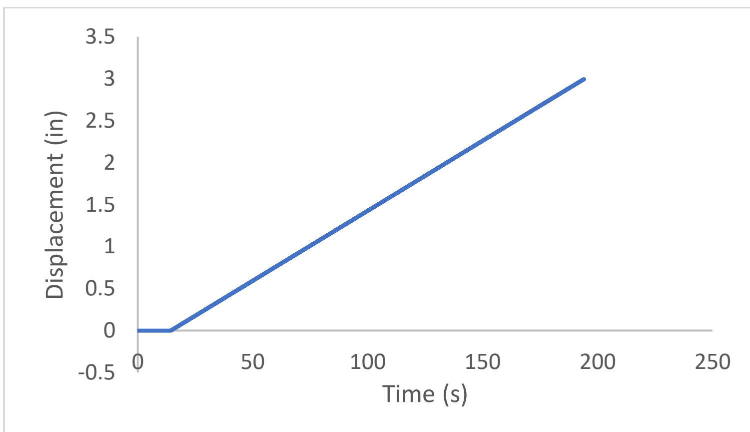

Figure 5.7 Plot of Displacement vs. Time. The maximum deflection was 3.00”.

The mass of the box beam was measured at 3.168 lb (Fig.5.8). This is less than the predicted weight of 3.59 lb. This is most likely because the mass lost from drilling holes for rivets was not taken into account in the predicted mass. The final strength-to-weight ratio of the box beam was 184.7, which is significantly more the predicted ratio. This is likely due to the significantly lower mass in the actual box beam.

Figure 5.8 Box beam weight measurement.

Table 5.1 summarizes the predicted and calculated values discussed above.

Table 5.1 Predicted VS. Experimental Values

Property	Predicted	Actual	Percent Error (%)
Mass	3.59 lbm	3.168 lbm	13.3
Failure Load	500 lbf	585.4 lbf	14.5
Deflection	0.03842 in	3.00 in	$7.7\text{x}10^3$
Strength-to-Weight Ratio	139.1	184.7	24.7

The percent error for the mass, failure load, and the strength-to-weight ratio are all more or less withn a nominal range with slight deviations such that the observed values in the strength-to weight ratio and fialure load case exceeded the preducted and fell short in the mass case. In the case of the deflection however the deflection that is much larger than the predicted is likely due to the fact that as the bold was pulled in greater and greater tension the box beam did more pitching forward than bending. What this means is that relative to own axis the box beam did not exerience much deflection but relative to the displacement induced by the crosshead the deflection was large.

As Group 1, the box beam was the 3rd best in terms of strength-to-weight ratio, and withstood the highest load (Fig.5.9)

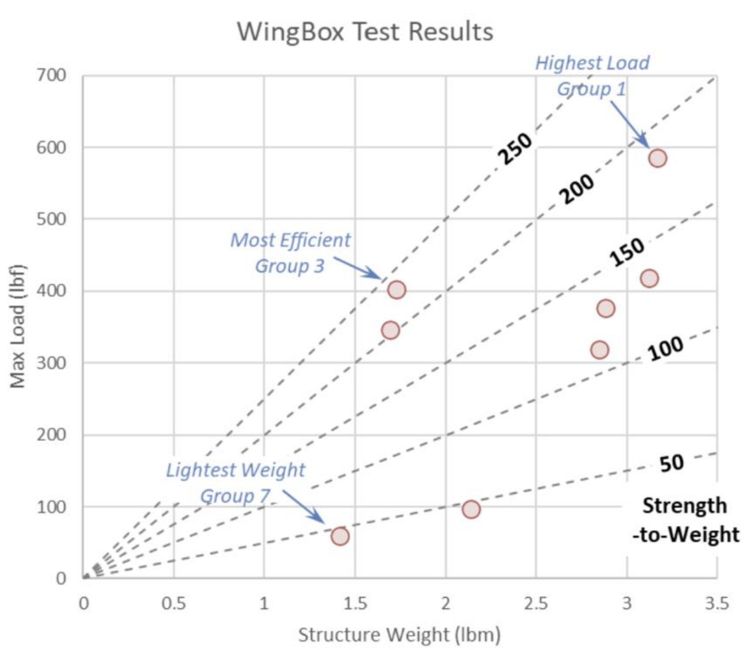

Figure 5.9 WingBox test results in comparison with other groups

6. DESIGN AND ANALYSIS CHANGES

The failure load from the test was greater than what was predicted. In the prediction analysis, many assumptions were made to make the analysis simpler. One assumption was that the torsional load would be maximized by placing the point load at the corner of the Wing Box. In the actual test, the point load was only 5/8” from the center instead of 3” from the center. This would decrease the torsional load on the Wing Box, changing the resulting shear stresses in the Wing Box from the two-cell box beam analysis.

A second assumption was that the skins were flat against the sides and tops of the box beam. This was not actually the case since the spars were made into C-channels to allow for fastening. This results in the addition of extra area to the lumped stringers and leads to a decreased axial loading on each node. This in turn increases the failure load to more closely match the actual test.

A third assumption was that the mass lost from the drilling of holes for rivets was negligible. Due to the thickness of the spars and the number and size of the holes, the mass lost was significant and the new analysis takes this into account when calculating the mass of the box beam.

The last assumption that was corrected in the new analysis is that the height of the box is assumed to be exactly 2 in. When measuring the height of the box, the actual height turns out to be 2.1in which is still within the tolerance. This additional height, while seemingly insignificant, means that the z-locations of each lumped stringer is further from the center of gravity and increases the moment of inertia of the wing box. This in turn leads to a lower axial stress due to the equation for bending stress. The lower axial stress enables the failure load to be increased.

By correcting these assumptions in the analysis, the predicted failure load becomes 550 lbf, the mass becomes 3.05 lbm, the strength-to-weight ratio becomes 182.0, and the safety factors when using the design load become what is shown in Table 6.1. The comparison of the old analysis results, new analysis results, and actual results is shown in Table 6.2. The new analysis predictions are very close to the actual results.

Table 6.1 Minimum Safety Factors for Design Load

Component	Load Type	Failure Mode	Safety Factor	Section
Top Skin	Shear	Yield Strength	8.73	Root
Top Skin	Shear	Ultimate Strength	8.01	Root
Bottom Skin	Shear	Yield Strength	6.98	Root
Bottom Skin	Shear	Ultimate Strength	8.01	Root
Bottom Skin	Compressive	Buckling	9.17	Root
Spar	Shear	Yield Strength	5.70	Root
Spar	Shear	Ultimate Strength	6.54	Root
Web	Shear	Yield Strength	33.07	Root
Web	Shear	Ultimate Strength	56.92	Root
Web	Shear	Buckling	81.3	Web
Top Spar Cap	Tensile	Yield Strength	48.03	Root
Top Spar Cap	Tensile	Ultimate Strength	43.18	Root
Top Spar Cap	Bearing	Joint	7.56	Root
Top Spar Cap	Net-Section	Joint	7.04	Root
Top Spar Cap	Shear-Out	Joint	7.21	Root
Bottom Spar Cap	Compressive	Yield Strength	27.81	Root
Bottom Spar Cap	Compressive	Buckling	10.25	Root
Top Clip	Tensile	Yield Strength	48.03	Root
Top Clip	Tensile	Ultimate Strength	43.18	Root
Bottom Clip	Compressive	Yield Strength	27.81	Root
Bottom Clip	Compressive	Buckling	45.69	Root
Bolt	Shear	Joint	102.99	Root
Rivet	Shear	Joint	12.47	Root

Table 6.2 Original Predictions, Adjusted Predictions, and Results Comparison

Property	Original Prediction	New Prediction	Actual	New Percent Error (%)
Mass	3.59 lbm	3.05 lbm	3.168 lbm	3.7
Failure Load	500 lbf	555 lbf	585.4 lbf	5.1
Strength-to-Weight Ratio	139.1	182.0	184.7	1.5

The objective of this project was to construct a Wing Box with the highest strength-to-weight ratio. The overall resistance to point loads, distributed loads, and bending moments was evident in the miniscule overall angle of twist observed and deflection. Had there not been the unexpected fastener shear as a function of the improper interdigitation of the threads the maximum sustained load would have increased. An area of improvement in the design is to ensure the alignment of the holes. Drilling the holes together will ensure that the holes are aligned for proper fastening which would eliminate the possibility of the fastener failure.

With the objective of maximizing the strength to weight ratio in mind, reducing the amount of clips to only two clips on the bottom and no clips on the top would have maintained the vertical bending strength while decreasing the weight of the design. The strength decrease from removing the clips is significant, but the removing of two clips also significantly reduces the weight.

The web could also be entirely removed. With the point load being 5/8” off center, the torsional load is small. Due to the test having minimal torsional load, the web, which mostly resists torsion, would not significantly assist in the overall wing box strength. The lack of torsional loads in the tests meant the design was overly designed which decreases our strength-to-weight ratio. The web added unnecessary weight to the design.

Another consideration is to add an additional rib. In the test, there was some buckling of the skin panel. The addition of an extra rib would help with this issue and reduce the buckling in the skin panel.

Additionally, we may want to consider tapering the design to make it lighter while having the root the same dimensions it currently carries. This will be beneficial as it will carry similar load capabilities with less weight, which is the main objective with aerospace structures. Moreover, the air drag will decrease with the taper design which would decrease the load applied to the Wing Box while in actual use.

7. CONCLUSIONS

When designing and manufacturing the Wing Box structure, we realized the importance of the different components that make up a Wing Box structure. Introducing components such as the spar caps, ribs, skins, and webs can drastically support the structure under loading while keeping the weight at a minimum. Going deeper into failure analysis, the following table can be formulated to see where failure is most likely to occur under the loading conditions.

Table 7.1 Safety Factors for Failure Load Most Likely to Occur

Component	Load Type	Failure Mode	Safety Factor	Section
Spar	Shear	Yield Strength	1.08	Root
Top Spar Cap	Bearing	Joint	1.07	Root
Top Spar Cap	Net-Section	Joint	1.00	Root
Top Spar Cap	Shear-Out	Joint	1.02	Root

As the safety factor approaches closer to 1, the failure mode becomes the most likely case of failure for the Wing Box. As shown in Table 7.1, Net-Section on the Top Spar Cap by the root is to fail first. This is evident as the Wing Box had undergone plastic deformation in the same fashion as predicted, which supports the analysis done. Understanding this, future designs can be created with increased emphasis on joint failure and possible Net-Section at the joint.

Apart from the design of the Wing Box, the manufacturing aspect of creating a Wing Box proved to be a valuable experience. From planning how to go about manufacturing the individual components to riveting and fastening everything together, the process of construing the Wing Box led itself to many challenges that are now understood better and can be tackled more effectively in the future. The main defect of our Wing Box was the drilled holes not being perfectly concentric which led to the bolt not being able to be completely fastened. Considering such parameters for future designs will yield more structurally sound Box Beams that can handle much more load.

8. REFERENCES

1. WingBox Structure Specification Rev-.doc
2. MMPDS-01.pdf
3. Niu, Chunyun. (2011). Airframe stress analysis and sizing. Hong Kong : Los Angeles, Calif. :Conmilit Press ; Technical Book Co. [distributor],
4. www.boltdepot.com